

# Simultaneous $T_1$ and $T_2$ Brain Relaxometry in Asymptomatic Volunteers Using Magnetic Resonance Fingerprinting

Chaitra Badve<sup>1</sup>, Alice Yu<sup>2</sup>, Matthew Rogers<sup>2</sup>, Dan Ma<sup>3</sup>, Yiying Liu<sup>4</sup>, Mark Schluchter<sup>4</sup>, Jeffrey Sunshine<sup>1</sup>, Mark Griswold<sup>1,3</sup>, and Vikas Gulani<sup>1,3</sup>

<sup>1</sup>Department of Radiology, Case Western Reserve University and University Hospitals, Cleveland, OH and <sup>2</sup>School of Medicine, Case Western Reserve University, Cleveland, OH, <sup>3</sup>Department of Biomedical Engineering, Case Western Reserve University and University Hospitals, Cleveland, OH and <sup>4</sup>Department of Biostatistics and Bioinformatics Core, Case Western Reserve University and University Hospitals, Cleveland, OH

## Corresponding Author:

Vikas Gulani

Department of Radiology, Case Western Reserve University and University Hospitals of Cleveland, 11100 Euclid Ave, Cleveland, OH 44106; E-mail: vikas@case.edu

**Key Words:** aging,  $T_1$  mapping,  $T_2$  mapping, magnetic resonance fingerprinting, relaxometry

**Abbreviations:** Cerebral spinal fluid (CSF), corpus callosum (CC), diffusion tensor imaging (DTI), echo time (TE), magnetic resonance fingerprinting (MRF), magnetic resonance imaging (MRI), region of interest (ROI), repetition time (TR), substantia nigra (SN), white matter (WM)

## ABSTRACT

Magnetic resonance fingerprinting (MRF) is an imaging tool that produces multiple magnetic resonance imaging parametric maps from a single scan. Herein we describe the normal range and progression of MRF-derived relaxometry values with age in healthy individuals. In total, 56 normal volunteers (24 men and 32 women) aged 11-71 years were scanned. Regions of interest were drawn on  $T_1$  and  $T_2$  maps in 38 areas, including lobar and deep white matter (WM), deep gray nuclei, thalami, and posterior fossa structures. Relaxometry differences were assessed using a forward stepwise selection of a baseline model that included either sex, age, or both, where variables were included if they contributed significantly ( $P < .05$ ). In addition, differences in regional anatomy, including comparisons between hemispheres and between anatomical subcomponents, were assessed by paired  $t$  tests. MRF-derived  $T_1$  and  $T_2$  in frontal WM regions increased with age, whereas occipital and temporal regions remained relatively stable. Deep gray nuclei such as substantia nigra, were found to have age-related decreases in relaxometry. Differences in sex were observed in  $T_1$  and  $T_2$  of temporal regions, the cerebellum, and pons. Men were found to have more rapid age-related changes in frontal and parietal WM. Regional differences were identified between hemispheres, between the genu and splenium of the corpus callosum, and between posteromedial and anterolateral thalami. In conclusion, MRF quantification measures relaxometry trends in healthy individuals that are in agreement with the current understanding of neurobiology and has the ability to uncover additional patterns that have not yet been explored.

## INTRODUCTION

Physiological aging changes in cerebral gray and white matter (WM) have been well documented in the neurobiology literature. Normal aging is associated with dendritic pruning, axonal loss, demyelination, and synaptic and neuronal loss (1-4). Several magnetic resonance imaging (MRI)-based metrics such as diffusion tensor imaging (DTI), diffusion, volumetry, and magnetization transfer ratio have been utilized to quantify age-related changes (5-13). MRI relaxometry techniques have also been used to quantify age-related changes in  $T_1$ ,  $T_2$ , and  $T_2^*$  relaxation properties in healthy individuals (14-23). To our knowledge, all relaxometry studies thus far have utilized separate sequences for quantifying 1 relaxation property at a time by measuring the signal recovery after spin inversion ( $T_1$ ) or the decay of the measured MRI signal ( $T_2$  or  $T_2^*$ ). Such experiments typically

suffer from long acquisition times and limited accuracy, which can limit utility.

Magnetic resonance fingerprinting (MRF) is a recently introduced method that simultaneously and rapidly measures multiple tissue properties, with initial application in measuring  $T_1$ , and  $T_2$ . This technique is based on the premise that acquisition parameters can be varied in a pseudorandom manner such that each combination of tissue properties will have a unique signal evolution. Using the Bloch equations, a dictionary of all possible signal evolutions can be created that includes all known acquisition parameters and all possible ranges of values and combinations of the properties of interest. The actual signal evolution in each voxel can then be compared to the dictionary entry, and the best dictionary match yields the property values for that voxel (24).

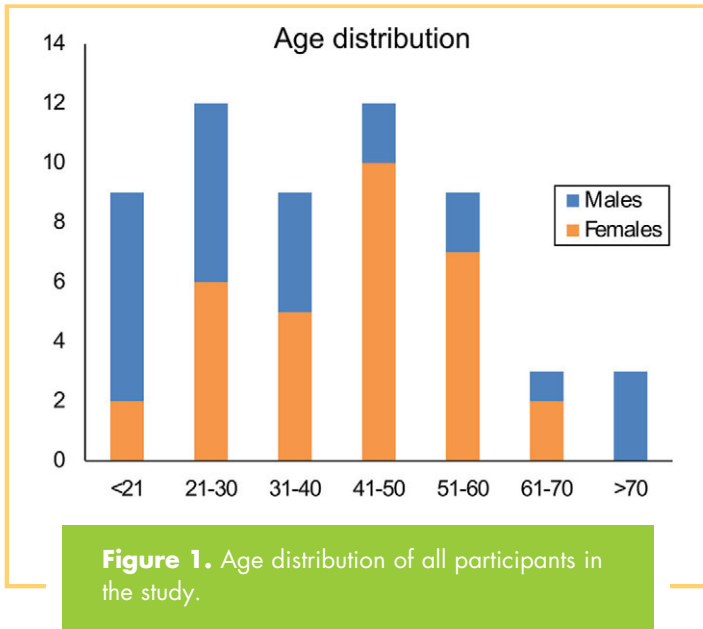


**Figure 1.** Age distribution of all participants in the study.

With MRF there is now the possibility of observing small changes in multiple tissue relaxation properties simultaneously. However, to date, no study to our knowledge has been performed to describe the normal range and progression of MRF-derived relaxometry values in healthy individuals. In this study, we present simultaneous quantification of regional brain T<sub>1</sub> and T<sub>2</sub> relaxation times in healthy volunteers using MRF and assess differences in tissue properties resulting from age, sex, and laterality of hemispheres. We further compare different best-fit options for regression analysis of age and brain relaxometry and assess how age-sex interactions affect these findings in the context of the known literature on relaxometry measurements with aging.

## METHODOLOGY

### Participant Recruitment

Informed written consent was obtained from all participants according to the protocol approved by the local institutional review board. Multislice MRF data were acquired in 56 healthy volunteers aged 11–71 years. There were 24 men (aged 11–71 years) and 32 women (aged 18–63 years), with an overall median age of 39 years (Figure 1). Of these participants, 53 were right-handed. One of the participants had a remote history of craniotomy for excising a meningioma; another had a remote history of surgical correction for Chiari 1 malformation. No other participant had a history of structural neurological disease or a known psychiatric disease. None of the participants revealed any overt parenchymal abnormalities on clinical T<sub>2</sub>-weighted images in the analyzed regions.

### MRF Acquisition

MRF scans were obtained on 3.0-T Verio and Skyra scanners (Siemens Healthcare, Erlangen, Germany) using standard 20-channel head coils. The acquisition technique has been previously described in detail (24). The parameters in MRF are continuously changed throughout the acquisition to create the desired spatial and temporal incoherence. The flip angle, phase,

repetition time (TR), echo time (TE), and sampling patterns are all varied in a pseudorandom fashion (24). The parameters used for MRF acquisition were as follows: field of view, 300 × 300 mm<sup>2</sup>; matrix size, 256 × 256; slice thickness, 5 mm; flip angle, 0–60°; TR, 8.7–11.6 ms; and radiofrequency pulse, sinc pulse with a duration of 800 μs and time-bandwidth product of 2. In a total acquisition time of 30.8 s, 3000 images were acquired for each slice. The TE was half of TR and varied with each TR. The MRF acquisition was planned on whole-brain clinical standard T<sub>2</sub>-weighted images that were acquired as follows: TR, 5650 ms; TE, 94 ms; FOV, 230 mm; slice thickness, 4 mm; and flip angle, 150°. Approximately 4–5 2D MRF slices were acquired through the whole brain for each individual depending on the head position. The entire study for each volunteer, including positioning time, was approximately 10 min in duration.

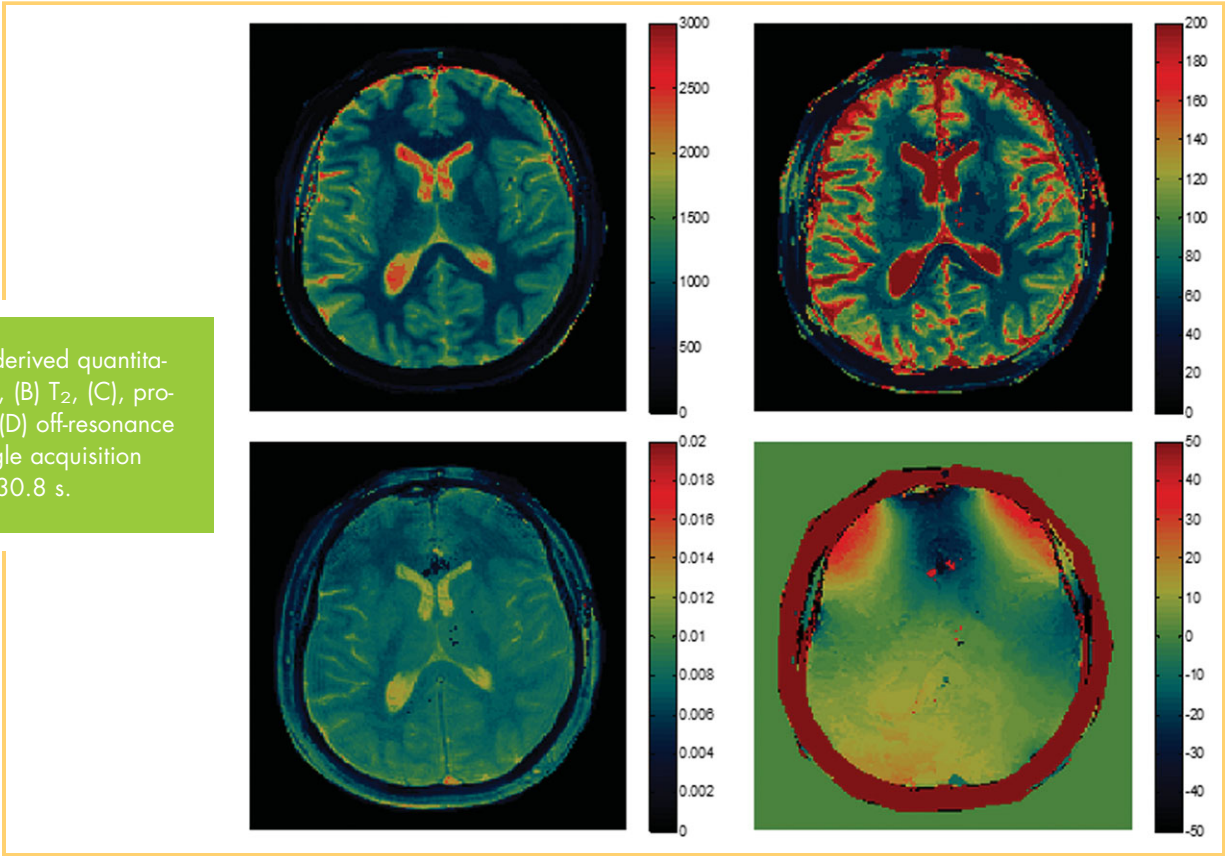
### Data Processing

Using simulation, a dictionary of signal evolutions that could arise from all possible combinations of materials or system-related properties was generated. A total of 287 709 signal time courses, each with 3000 time points and different sets of T<sub>1</sub>, T<sub>2</sub>, and off-resonance parameters, were simulated for the dictionary. The ranges of T<sub>1</sub> and T<sub>2</sub> were chosen according to the typical physiological ranges of the tissues in the brain. T<sub>1</sub> values between 100 and 3000 ms and T<sub>2</sub> values between 10 and 500 ms were included in the dictionary. The off-resonance values included the range between –400 and 400 Hz. The total simulation time was 5.3 min. The vector dot product between the measured signal and each dictionary entry was calculated, and the entry yielding the highest dot product was selected as the closest match to the acquired signal (14). The final output consisted of quantitative T<sub>1</sub>, T<sub>2</sub>, off-resonance, and proton-density maps (Figure 2). MRF-based proton-density values are affected by the type of acquisition as well as the sensitivity of the receiver coil and thus are not purely tissue-specific. Therefore, only T<sub>1</sub> and T<sub>2</sub> maps were utilized for further anatomical analysis.

### Data Analysis

All data processing and analysis were performed using MATLAB version R2013b (MathWorks, Natick, MA) and SAS version 9.4 (SAS Institute, Inc, Cary NC). A region of interest (ROI)-based analysis was performed on the relaxometry maps as follows. For every subject, a fellowship-trained neuroradiologist manually drew the ROIs from which mean T<sub>1</sub> and T<sub>2</sub> measures were extracted. A total of 38 ROIs (17/hemisphere plus 4 midline) were drawn for each subject (Figure 3). The selected regions constituted important WM regions, deep gray nuclei, and posterior fossa structures. Cortical gray matter was not studied to avoid partial volume effects from cerebral spinal fluid (CSF) and WM. T<sub>1</sub> and T<sub>2</sub> maps with narrow window settings and magnified views were used to clearly identify each anatomical region and draw the ROIs. The ROI size depended on the region analyzed and ranged from 4 to 10 mm<sup>2</sup>. Caution was taken to place the ROI in the center of the sampled region, with careful separation from adjacent structures to avoid partial volume effects. Regions with grossly visible artifacts or distortion were excluded from measurements.

**Figure 2.** MRF-derived quantitative maps. (A) T<sub>1</sub>, (B) T<sub>2</sub>, (C), proton density, and (D) off-resonance maps from a single acquisition with duration of 30.8 s.



**Statistical Analysis**

T<sub>1</sub> and T<sub>2</sub> values extracted from the MRF data were analyzed based on a review of the literature. Previous relaxometry studies have utilized either a linear or polynomial regression model to assess the relation between age and relaxometry (14–23). For this study, age and sex effects were first examined using forward stepwise selection to select a baseline model that included either age, sex, or both, where variables were included at each step if they were significant with a *P* value <.05. For regions where the baseline model included age, we then tested whether adding a quadratic term to the model significantly (*P* < .05) improved fit.

In addition, for regions with significant linear age effects, effects in men and women were compared using a test of equality between slopes to assess for age and sex interaction. Based on the slopes and intercepts, age-sex interplay was categorized as either an age + sex effect or age × sex effect. The age + sex effect included regions where men and women had similar slopes with respect to age but different intercepts. The age × sex effect included regions where each sex had significantly different slopes and intercepts with respect to age. Thus, for each brain region, we evaluated changes of MRF-based T<sub>1</sub> and T<sub>2</sub> with age using linear and quadratic models, differences between

**Figure 3.** ROI locations. (A) 1, superior frontal white matter; 2, centrum semiovale. (B) 3, frontal WM; 4, caudate nucleus; 5, putamen; 6, globus pallidus; 7, medial thalamus; 8, lateral thalamus; 9, internal capsule; 10, genu; 11, splenium; 12, parietal WM. (C) 13, substantia nigra; 14, red nucleus; 15, temporal WM; 16, occipital WM. (D) 17, middle cerebellar peduncle; 18, cerebellum; 19, dentate nucleus; 20, vermis; 21, pons.

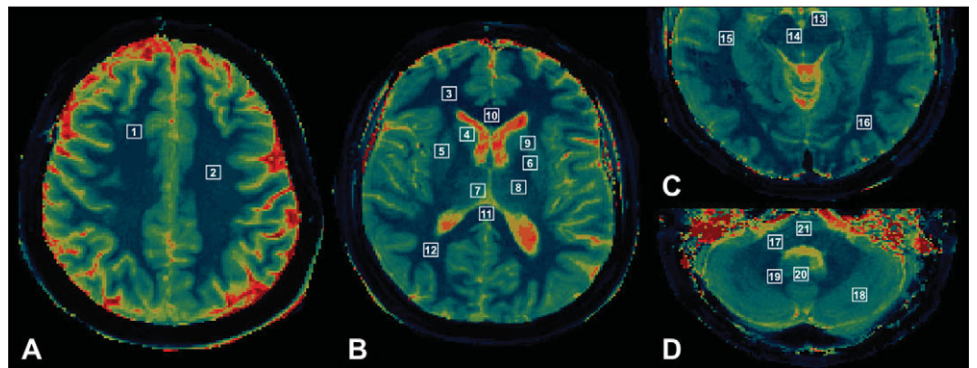


**Table 1.** Regions Showing Significant Linear Relation Between Relaxation Parameters and Age Without Any Sex Effects

| Region Name                         | Intercept | Slope   | P                  | R <sup>2</sup> |
|-------------------------------------|-----------|---------|--------------------|----------------|
| <b>T<sub>1</sub> relaxometry</b>    |           |         |                    |                |
| Right superior frontal white matter | 821.98    | 0.848   | .045               | 0.07           |
| Right centrum semiovale             | 843.14    | 1.179   | .010               | 0.11           |
| Left centrum semiovale              | 850.49    | 1.081   | .029               | 0.08           |
| Corpus callosum genu                | 743.60    | 1.086   | .029               | 0.12           |
| Left substantia nigra               | 976.9     | -2.893  | .0004 <sup>a</sup> | 0.24           |
| <b>T<sub>2</sub> relaxometry</b>    |           |         |                    |                |
| Left frontal white matter           | 58.64     | 0.1840  | .0002 <sup>a</sup> | 0.24           |
| Left thalamus (medial)              | 59.21     | 0.1071  | .0299              | 0.09           |
| Right substantia nigra              | 46.21     | -0.1090 | .015               | 0.13           |
| Left substantia nigra               | 47.29     | -0.1321 | .011               | 0.13           |

<sup>a</sup> Statistically significant after correcting for multiple comparison testing using the Bonferroni method.

ing using the Bonferroni method was also utilized, and outcomes that were statistically significant overall were identified.

**RESULTS**

All regions with field inhomogeneity and susceptibility artifacts were excluded from analysis. The largest number of field inhomogeneity and banding artifacts was seen in the genu region of the CC (n = 15). T<sub>2</sub> maps were more susceptible to field inhomogeneity artifacts compared with T<sub>1</sub>. Although we did our best to include all ROIs in the collected slices, slight variations in slice placement during imaging resulted in the omission of some regions, most commonly the splenium of the CC (n = 8).

**Aging Progression**

When examining T<sub>1</sub>, positive linear correlations with age were observed in 3 frontal WM regions and the genu of the CC. Negative linear correlations were seen in the left substantia nigra (SN) (Table 1 and Figure 4A). Quadratic trends were observed in 3 fronto-parietal WM regions and the right SN, with the latter showing an overall decline in T<sub>1</sub> with age (Table 2 and Figure 4B). When examining T<sub>2</sub>, positive linear correlations were seen in left frontal WM and the medial left thalamus, whereas negative linear correlations with age were detected in the bilateral SN (Table 1 and Figure 4A). Quadratic relationships with age were observed in right frontal WM and the left dentate nucleus, with an additional effect on sex in right frontal WM described further in the following section (Table 2 and Figure 4B).

**Differences Between Sexes**

Differences in MRF-derived relaxometry between sexes were observed in the absence of a significant correlation with age. Of the 38 regions examined in the T<sub>1</sub> analysis, left temporal WM, bilateral cerebellar hemispheres, and pons showed differences between sexes, with a higher T<sub>1</sub> in men compared with women and no significant change with age. In the T<sub>2</sub> analysis, a significant difference between sexes was detected in the right lentiform nucleus.

Differences between sexes with age effects were categorized as either an age + sex effect (men and women had similar slopes

sexes, and differences in the trajectory of age effects between sexes.

To test for differences between right and left hemispheres, regional relaxometry data from only right-handed participants (n = 53) were used. In this subanalysis, a paired t test was performed to compare relaxometry measures for each region across hemispheres. A paired t test was also used to compare different components within a region, specifically between the medial and lateral thalami and between the genu and splenium of the corpus callosum (CC). For this subgroup analysis, pooled data from right- and left-handed subjects were analyzed.

For statistical analysis, all comparisons with a P value <.05 before correcting for multiple comparisons were considered significant results and discussed. This was done with the intention of describing all identifiable trends that may have physiological implications. However, correcting for multiple comparison test-

**Figure 4.** Regions with significant T<sub>1</sub> and T<sub>2</sub> correlation with age. (A) Regions with a significant linear relationship between T<sub>1</sub>, T<sub>2</sub>, and age. (B) Regions with a significant quadratic relation between relaxation parameters and age.

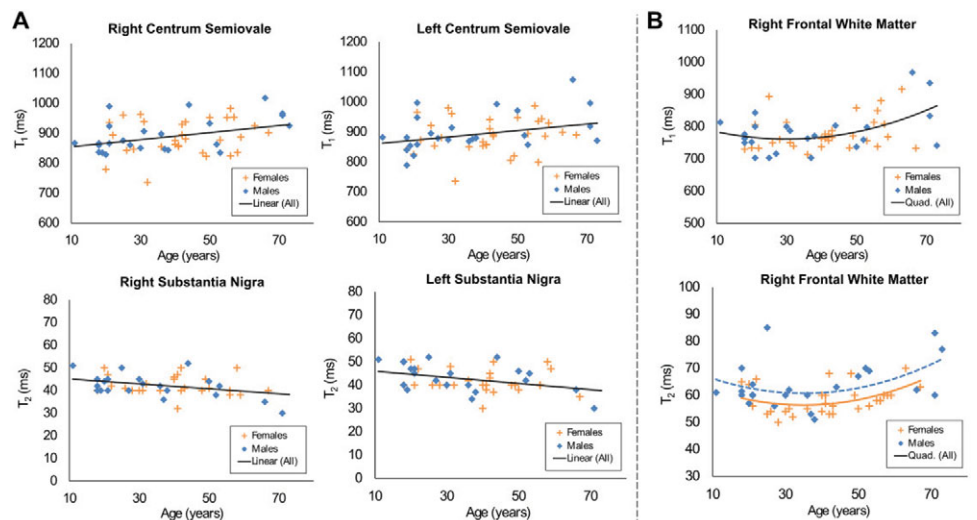


**Table 2.** Regions Showing Significant Quadratic Relation Between Relaxation Parameters and Age

| Region Name                             | Intercept | Age     | Age <sup>2</sup> | P(age) <sup>2</sup> | R <sup>2</sup> |
|---|-----------|---------|------------------|---------------------|----------------|
| T <sub>1</sub> relaxometry              |           |         |                  |                     |                |
| Right frontal white matter              | 811.8     | -3.3619 | 0.0559           | .045                | 0.21           |
| Left frontal white matter               | 848.3     | -4.4117 | 2.3849           | .021                | 0.19           |
| Left parietal white matter              | 905.5     | -5.5573 | 0.0928           | .001 <sup>b</sup>   | 0.42           |
| Right substantia nigra                  | 1093.8    | -10.287 | 0.0965           | .008 <sup>b</sup>   | 0.39           |
| T <sub>2</sub> relaxometry              |           |         |                  |                     |                |
| Right frontal white matter <sup>a</sup> | 67.18     | -0.6168 | 0.0088           | .013                | 0.32           |
| Women                                   | 67.18     | -0.6168 | 0.0088           | .013                | 0.32           |
| Men                                     | 71.52     | -0.6168 | 0.0088           |                     |                |
| Left dentate nucleus                    | 74.62     | -0.6124 | 0.0060           | .046                | 0.16           |

<sup>a</sup> For right frontal white matter, the quadratic model also included a term for sex, which was statistically significant ( $P = 0.023$ ), indicating a difference in intercepts between men and women. Results are displayed as separate regressions for men and women having different intercepts but the same linear and quadratic terms for age.

<sup>b</sup> Statistically significant after correcting for multiple comparison testing using the Bonferroni correction technique.

with respect to age but different intercepts) or age × sex effect (men and women had significantly different slopes and intercepts). Recall that age effects could be fit with a linear or quadratic model. In the T<sub>1</sub> analysis, left superior frontal and right parietal WM showed a linear age + sex effect (Figure 5A). In the T<sub>2</sub> analysis, age × sex interaction was seen in bilateral superior frontal and parietal WM and the centrum semiovale. A linear age + sex effect was observed in right superior frontal WM, and a quadratic age + sex effect was observed in right frontal WM and the right dentate nucleus (Figure 5B).

Of all the sex differences measured, after adjusting for multiple comparison testing, only T<sub>1</sub> variations in right parietal WM ( $P < .0001$ ,  $R^2 = 0.30$ ) and T<sub>2</sub> differences in right superior frontal WM ( $P < .0001$ ,  $R^2 = 0.30$ ) remained statistically significant.

**Regional Differences**

Only right-handed individuals ( $n = 53$ ) were included in this analysis, and 34 paired regions were studied. Several regions with T<sub>1</sub> and T<sub>2</sub> differences between right and left hemispheres

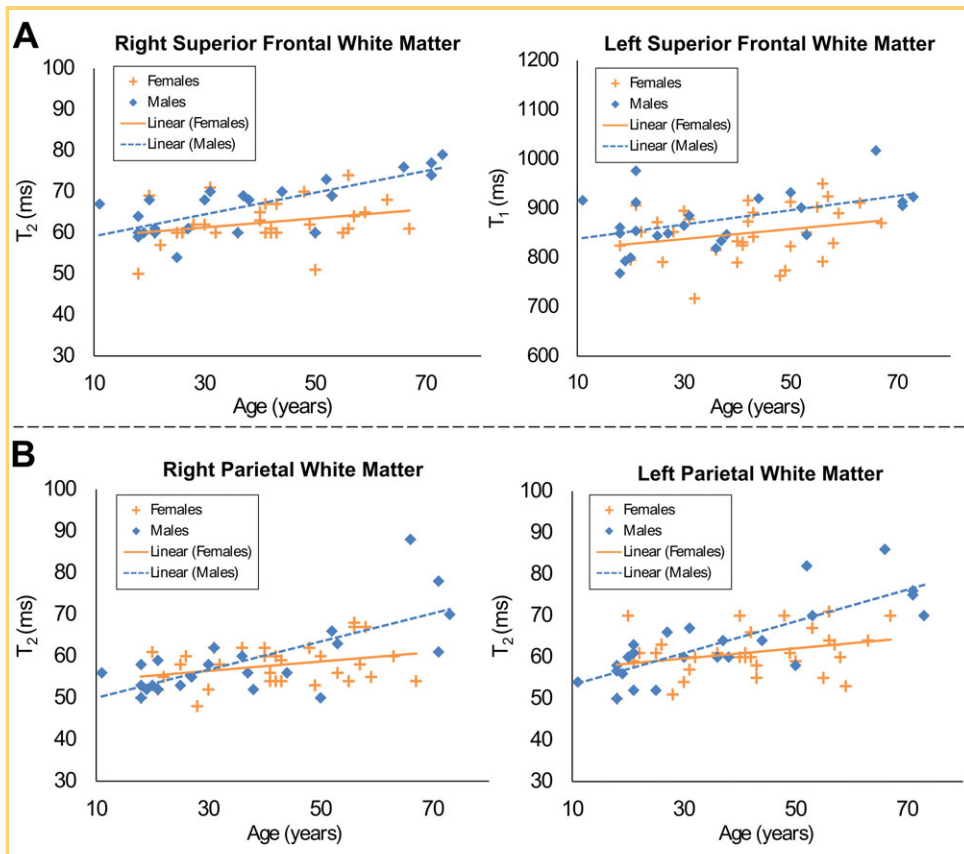


**Figure 5.** Regions with significant age and sex effects. (A) Regions with significant linear age + sex effects; in these models, the slope of linear regression on age for men and women is similar but the intercepts are significantly different. (B) Regions with significant age × sex effect on T<sub>2</sub> relaxometry; in this model, the slope of linear regression on age between men and women is statistically significant.

**Table 3.** Relaxometry Differences Across Hemispheres and Within Regions

| Region                          | Differences Across Hemispheres <sup>a</sup> |        |       |                     |                |       |      |                     |
|---------------------------------|---|--------|-------|---------------------|----------------|-------|------|---------------------|
|                                 | T <sub>1</sub>                              |        |       |                     | T <sub>2</sub> |       |      |                     |
|                                 | n   | Mean   | SD    | P                   | n              | Mean  | SD   | P                   |
| Superior frontal white matter   | 53  | -6.29  | 25.97 | .083                | 52             | -1.35 | 3.81 | .013                |
| Centrum semiovale               | 52  | -2.98  | 28.03 | .446                | 52             | -1.63 | 3.81 | .003                |
| Frontal white matter            | 52  | -13.04 | 39.42 | .020                | 52             | -5.01 | 7.68 | <.0001 <sup>b</sup> |
| Caudate nucleus                 | 49  | -4.52  | 48.29 | .515                | 45             | 2.78  | 7.72 | .020                |
| Putamen                         | 52  | -17.00 | 40.32 | .003                | 51             | -1.98 | 5.22 | .009                |
| Parietal white matter           | 52  | 1.13   | 42.98 | .850                | 52             | -3.92 | 5.34 | <.0001 <sup>b</sup> |
| Internal capsule                | 50  | -14.52 | 33.02 | .003                | 48             | 2.99  | 7.21 | .006                |
| Occipital matter                | 48  | -17.98 | 56.58 | .032                | 48             | -3.52 | 5.88 | .0001 <sup>b</sup>  |
| Temporal white matter           | 45  | 33.02  | 58.97 | .0005 <sup>b</sup>  | 46             | -0.83 | 6.33 | .377                |
| Middle cerebellar peduncle      | 48  | 20.08  | 51.92 | .010                | 48             | -1.58 | 5.05 | .035                |
| Dentate nucleus                 | 47  | -6.44  | 48.71 | .369                | 45             | -4.11 | 4.96 | <.0001 <sup>b</sup> |
| Cerebellum                      | 49  | 2.72   | 69.67 | .785                | 47             | -3.48 | 7.02 | .001 <sup>b</sup>   |
| Region                          | Difference Within Structures <sup>c</sup>   |        |       |                     |                |       |      |                     |
|                                 | T <sub>1</sub>                              |        |       |                     | T <sub>2</sub> |       |      |                     |
|                                 | n   | Mean   | SD    | P                   | n              | Mean  | SD   | P                   |
| Right thalamus (medial-lateral) | 52  | 91.48  | 54.76 | <.0001 <sup>b</sup> | 51             | 4.55  | 5.35 | <.0001 <sup>b</sup> |
| Left thalamus (medial-lateral)  | 51  | 110.91 | 52.77 | <.0001 <sup>b</sup> | 51             | 6.72  | 4.40 | <.0001 <sup>b</sup> |
| Corpus callosum (genu-splenium) | 35  | -68.00 | 55.63 | <.0001 <sup>b</sup> | 35             | 4.37  | 7.34 | .0012 <sup>b</sup>  |

<sup>a</sup> Includes only right-handed participants.

<sup>b</sup> Statistically significant after correcting for multiple comparison testing using the Bonferroni correction technique.

<sup>c</sup> Includes right- and left-handed participants.

were identified (Table 3). In the analysis within regions, the splenium of the CC had a significantly higher T<sub>1</sub> but lower T<sub>2</sub> compared with the genu. The medial components of bilateral thalami showed higher T<sub>1</sub> and T<sub>2</sub> values compared with the lateral components.

## DISCUSSION

To our knowledge, this is the first in vivo use of MRF at 3.0 T for measuring tissue properties of multiple brain regions in healthy human subjects across different age groups. At a microstructural level, brain aging is characterized by the loss of myelinated fibers, myelin pallor, ballooning, and redundant myelination; at a macroscopic level, there is a loss of grey and WM volume and expansion of CSF spaces (25–28). An increase in free water and decrease in water bound to macromolecules (such as myelin) are reflected by a lower magnetization transfer ratio in older age groups (29, 30). The increase in gliosis, free water content, loss of myelination, and other aging changes also result in longer T<sub>1</sub> and T<sub>2</sub> relaxation times in WM. Although the published literature varies in the types of statistical modeling employed and regional predilection of findings, all studies to our knowledge agree that there is an overall increase in T<sub>1</sub> (1/R<sub>1</sub>) and/or T<sub>2</sub> (1/R<sub>2</sub>) in various WM regions/tracts with increasing age (31–33).

A recent study measured the R<sub>1</sub> of various WM tracts over age and found that it increased from childhood up to the age of

approximately 40 years and then decreased to 8-year-old levels between the ages of 70 and 80 years (13). In this study, comparable trends are seen in the T<sub>1</sub> of bilateral frontal and left parietal WM, with a dip in T<sub>1</sub> values between 30 and 50 years followed by an increase in later decades (Figure 4B and Table 2). Various volumetry and DTI studies have consistently demonstrated a frontal predilection for age-related changes (34–37). DeCarli et al. (34) also showed that the volumes of bilateral temporal lobes stayed stable across the human lifespan. These findings support the results shown herein that demonstrate that age effects on WM relaxometry are significant in frontal and parietal regions, whereas occipital and temporal relaxometry values stay relatively stable. In addition, the fact that the quadratic age model is a significantly better fit for certain frontal and parietal white regions over a linear age model alludes to a dynamic state of tissue turnover in these regions throughout the adult life.

WM in the genu of the CC also demonstrated increased T<sub>1</sub> with age in this study. Previous DTI and relaxometry studies that explored the effects of aging on CC microstructure have found that the anterior portions of the CC (including the genu) are more susceptible to age-dependent changes compared with the splenium (38–40). More specifically, DTI studies showed greater decreases in fractional anisotropy in the genu that were explained by increases in free water content and demyelination in

the CC with age. Such microstructural changes would also cause an increase in T<sub>1</sub> relaxometry (Table 2).

With age, deep gray nuclei show drops in T<sub>2</sub> and less frequently T<sub>1</sub> values secondary to increasing mineralization and iron deposition (13, 32, 33, 41, 42). We identified similar trends in the left dentate nucleus and bilateral SN, the latter being statistically significant. T<sub>2</sub> shortening in the SN can be explained by increasing iron deposition as part of the physiological aging process and has been extensively reported in the literature (43–47). On the other hand, the age-dependent decrease in T<sub>1</sub> of the SN has not been as extensively explored. A recent study that assessed the relation between R<sub>1</sub> of the SN and age showed findings similar to our results (48). Histopathological studies of the SN have shown that there is nearly a 10% decrease in the number of neuromelanin-containing neurons per decade in neurologically intact individuals (49). Because neuromelanin inherently has a T<sub>1</sub>-shortening effect, in theory this loss should manifest as T<sub>1</sub> lengthening with age, but the data indicate a different effect to be dominant. The findings seen here may be an outcome of the combination of iron deposition and extraneuronal melanin deposition that are also seen with normal aging, both of which are expected to shorten T<sub>1</sub> (44, 49–51). In this study, T<sub>1</sub> and T<sub>2</sub> in the SN were determined to decrease with age in a linear or quadratic pattern.

There is currently no consensus in the neuroimaging literature on whether a linear or quadratic model is the best fit for regression analysis of age and relaxometry. In addition, there is no physiologic reason to assume that the entire brain should conform to 1 model uniformly over the other. Our results suggest that for the more dynamically changing frontal WM regions, the quadratic model may be a better fit than the linear model, especially for T<sub>1</sub> (Figure 4B).

Two major differences in sex relaxometry were seen in this study, the first being different effects of aging on certain WM regions for men and women. In older age groups, men were observed to have higher relaxation time measurements in frontal and parietal WM compared with women. A few studies that looked at age and sex interactions in the past have shown that frontotemporal volume loss with age is more prominent in men, although a few other imaging studies have shown no such interaction (8, 52–55). Coffey et al. (56) found that there was a greater age-related increase in sulcal and Sylvian CSF volumes with a lower size of parietal-occipital regions in men compared with women. The effects that sex has on aging as seen in our study are an additional piece of evidence that could reflect the greater predilection of men toward neurodegenerative processes and neurocognitive decline, which become more prominent with age (56–58). The second major difference in sex relaxometry that was identified in this study was in the mean relaxometry of temporal regions, the cerebellum, and pons. Similar sex effects seen previously have been attributed to sexual dimorphism that arose from how sex steroids affected microscopic processes such as glial proliferation, myelination, the presence of paramagnetic substances, and macrostructural phenotypes of gray and WM volumes (7, 8, 32, 54, 59–61).

In right-handed subjects, several areas of hemispheric asymmetry were identified in frontal, parietal, and temporal WM, the internal capsule region, and dentate nuclei. These

regional differences hint at underlying microstructural distinctions that stem from asymmetry in the motor cortex and WM connectivity (62). Previous attempts to evaluate cerebral laterality with techniques such as morphometry, DTI, and functional MRI have shown that several subtle macro- and microstructural differences in cerebral hemispheres can be identified, although there is no single predominant pattern that has emerged (63–67).

In this study, the genu of the CC showed significantly lower T<sub>1</sub> and higher T<sub>2</sub> values compared with the splenium. Previous DTI studies have shown higher fractional anisotropy in the splenium of the CC compared with the genu region (68, 69). Thus, these 2 regions of the CC are known to have measurable differences on diffusion MRI. Several factors such as axonal fiber density, diameter of fibers, orientation, degree of myelination, and overall microstructural integrity that affect the diffusion metrics could also have an effect on the relaxometry characteristics of the CC and explain our findings, although the exact relation between these factors remains unexplored.

We also found interesting regional variation in thalami relaxometry. For this analysis, it was not possible to anatomically segment the thalami into the component nuclei. Rather than analyze each thalamus in its entirety, we divided it into posteromedial and anterolateral components. The posteromedial segment approximately included the regions of pulvinar and medial nuclei, whereas the anterolateral segment included the anterior and lateral regions. For both hemispheres, the T<sub>1</sub> and T<sub>2</sub> of posteromedial thalami were higher by approximately 100 and 5 ms, respectively, compared with the lateral portions. The exact cause of these differences is unclear, although a differential in gray-white matter composition, unique nuclear arrangement, and differences in associated WM pathways may explain some of these findings (70). Several relaxometry studies have been attempted in normal subjects and in patients with multiple sclerosis (41, 71, 72). Because thalami are frequently studied in multiple sclerosis, our findings could have implications in designing future relaxometry studies in patients, as it may be necessary to analyze the medial and lateral portions of the thalami separately.

This study utilized the original MRF technique with 2D acquisitions and an in-plane resolution of 1.2 mm (24). The lack of 3D whole-brain data limited the ability of selecting brain regions and necessitated analysis using the time-intensive ROI method. Future iterations of MRF acquisitions should seek to address these limitations with improved in-plane resolution and 3D acquisition capabilities while improving processing speeds and patient comfort (73, 74). Relaxometry measurements from certain regions such as the genu of the CC are limited by the presence of field inhomogeneity and banding artifacts. These artifacts are more typical for all types of balanced steady-state free precession-based sequences and are commonly seen near air-tissue interface, where large field inhomogeneity is introduced. The incidence of these artifacts could be considerably reduced in future studies by using the fast imaging with steady-state precession-based MRF acquisition technique (75).

Limitations of this study include the lack of details about study participant medical history that may affect brain anatomy and microstructure, including history of caffeine and alcohol intake, smoking, and diseases such as diabetes mellitus, hypertension, endocrinopathies, or current medications, and these

factors could potentially alter relaxation parameters. No minimal state examination or psychological testing was administered to the participants as part of this study, although all participants demonstrated understanding of the consent form. Our ROIs included deep gray nuclei and WM regions; cortical gray matter was not analyzed.

In conclusion, this pilot study introduces MRF as a rapid multiparametric *in vivo* quantitation tool in normative brain

imaging and demonstrates that it can identify and quantify differences in brain parenchyma related to age, sex, hemisphere, and anatomy. This T<sub>1</sub> and T<sub>2</sub> normative database can be used as a reference for future MRF studies in various disease states. Dedicated efforts to improve in-plane resolution, facilitate 3D coverage, and reduce inhomogeneity artifacts are underway to develop an efficient and powerful quantitation tool for applications in neuroimaging and beyond.

## ACKNOWLEDGMENTS

This research was funded by NIH grants 1R01EB016728, R01BB017219, and R01DK098503 and by Siemens Healthcare.

## REFERENCES

- Gunning-Dixon FM, Raz N. The cognitive correlates of white matter abnormalities in normal aging: a quantitative review. *Neuropsychology*. 2000;14(2):224–232.
- Gunning-Dixon FM, Brickman AM, Cheng JC, Alexopoulos GS. Aging of cerebral white matter: a review of MRI findings. *Int J Geriatr Psychiatry*. 2009;24(2):109–117.
- Kennedy KM, Raz N. Pattern of normal age-related regional differences in white matter microstructure is modified by vascular risk. *Brain Res*. 2009;1297:41–56.
- Pannese E. Morphological changes in nerve cells during normal aging. *Brain Struct Funct*. 2011;216(2):85–89.
- Ge Y, Grossman RI, Babb JS, Rabbin ML, Mannon LJ, Kolson DL. Age-related total gray matter and white matter changes in normal adult brain. Part II: quantitative magnetization transfer ratio histogram analysis. *AJNR Am J Neuroradiol*. 2002;23(8):1334–1341.
- Salat DH, Tuch DS, Greve DN, Van Der Kouwe AJW, Zaleta AK, Rosen BR, Fischl B, Corkin S, Rosas HD. Age-related alterations in white matter microstructure measured by diffusion tensor imaging. *Neurobiol Aging*. 2005;26(8):1215–1227.
- Raz N, Lindenberger U, Rodrigue KM, Kennedy KM, Head D, Williamson A, Dahle C, Gerstorf D, Acker JD. Regional brain changes in aging healthy adults: general trends, individual differences and modifiers. *Cereb Cortex*. 2005;15(11):1676–1689.
- Hsu JL, Leemans A, Bai CH, Lee CH, Tsai YF, Chiu HC, Chen WH. Gender differences and age-related white matter changes of the human brain: a diffusion tensor imaging study. *Neuroimage*. 2008;39(2):566–577.
- Michielse S, Coupland N, Camicioli R, Carter R, Seres P, Sabino J, Malychin N. Selective effects of aging on brain white matter microstructure: a diffusion tensor imaging tractography study. *Neuroimage*. 2010;52(4):1190–1201.
- Giorgio A, Santelli L, Tomassini V, Bosnell R, Smith S, De Stefano N, Johansen-Berg H. Age-related changes in grey and white matter structure throughout adulthood. *Neuroimage*. 2010;51(3):943–951.
- Westlye LT, Walhovd KB, Dale AM, Bjørnerud A, Due-Tønnessen P, Engvig A, Grydeland H, Tamnes CK, Ostby Y, Fjell AM. Life-span changes of the human brain white matter: diffusion tensor imaging (DTI) and volumetry. *Cereb Cortex*. 2010;20(9):2055–2068.
- Hedman AM, Van haren NE, Schnack HG, Kahn RS, Pol H, Hilleke E. Human brain changes across the life span: a review of 56 longitudinal magnetic resonance imaging studies. *Hum Brain Mapp*. 2012;33(8):1987–2002.
- Yeatman JD, Wandell BA, Mezer AA. Lifespan maturation and degeneration of human brain white matter. *Nat Commun*. 2014;5:4932.
- Agartz I, Säaf J, Wahlund LO, Wetterberg L. T<sub>1</sub> and T<sub>2</sub> relaxation time estimates in the normal human brain. *Radiology*. 1991;181(2):537–543.
- Breger RK, Yetkin FZ, Fischer ME, Papke RA, Haughton VM, Rimm AA. T<sub>1</sub> and T<sub>2</sub> in the cerebrum: correlation with age, gender, and demographic factors. *Radiology*. 1991;181(2):545–547.
- Callaghan MF, Freund P, Draganski B, Anderson E, Cappelletti M, Chowdhury R, Diedrichsen J, FitzGerald TH, Smittenaar P, Helms G. Widespread age-related differences in the human brain microstructure revealed by quantitative magnetic resonance imaging. *Neurobiol Aging*. 2014;35(8):1862–1872.
- Cho S, Jones D, Reddick WE, Ogg RJ, Steen RG. Establishing norms for age-related changes in proton T<sub>1</sub> of human brain tissue *in vivo*. *Magn Reson Imaging*. 1997;15(10):1133–1143.
- Saito N, Sakai O, Ozonoff A, Jara H. Relaxo-volumetric multispectral quantitative magnetic resonance imaging of the brain over the human lifespan: global and regional aging patterns. *Magn Reson Imaging*. 2009;27(7):895–906.
- Siemonsen S, Finsterbusch J, Matschke J, Lorenzen A, Ding XQ, Fiehler J. Age-dependent normal values of T<sub>2</sub> and T<sub>2</sub>' in brain parenchyma. *AJNR Am J Neuroradiol*. 2008;29(5):950–955.
- Steen RG, Gronemeyer SA, Taylor JS. Age-related changes in proton T<sub>1</sub> values of normal human brain. *J Magn Reson Imaging*. 1995;5(1):43–48.
- Steen RG, Ogg RJ, Reddick WE, Kingsley PB. Age-related changes in the pediatric brain: quantitative MR evidence of maturational changes during adolescence. *AJNR Am J Neuroradiol*. 1997;18(5):819–828.
- Suzuki S, Sakai O, Jara H. Combined volumetric T<sub>1</sub>, T<sub>2</sub> and secular-T<sub>2</sub> quantitative MRI of the brain: age-related global changes (preliminary results). *Magn Reson Imaging*. 2006;24(7):877–887.
- Vymazal J, Righini A, Brooks RA, Canesi M, Mariani C, Leonardi M, Pezzoli G. T<sub>1</sub> and T<sub>2</sub> in the brain of healthy subjects, patients with Parkinson disease, and patients with multiple system atrophy: relation to iron content. *Radiology*. 1999;211(2):489–495.
- Ma D, Gulani V, Seiberlich N, Liu K, Sunshine JL, Duerk JL, Griswold MA. Magnetic resonance fingerprinting. *Nature*. 2013;495(7440):187–192.
- Peters A. The effects of normal aging on myelin and nerve fibers: a review. *J Neurocytol*. 2002;31(8–9):581–593.
- Bartzokis G. Age-related myelin breakdown: a developmental model of cognitive decline and Alzheimer's disease. *Neurobiol Aging*. 2004;25(1):5–18.
- Raz N, Rodrigue KM. Differential aging of the brain: patterns, cognitive correlates and modifiers. *Neurosci Biobehav Rev*. 2006;30(6):730–748.
- Sala S, Agosta F, Pagani E, Copetti M, Comi G, Filippi M. Microstructural changes and atrophy in brain white matter tracts with aging. *Neurobiol Aging*. 2012;33(3):488–498.e2.
- Fazekas F, Ropele S, Enzinger C, Gorani F, Seewann A, Petrovic K, Schmidt R. MTL of white matter hyperintensities. *Brain*. 2005;128(Pt 12):2926–2932.
- Spilt A, Geeraedts T, De Craen AJ, Westendorp RG, Blauw GJ, van Buchem MA. Age-related changes in normal-appearing brain tissue and white matter hyperintensities: more of the same or something else? *AJNR Am J Neuroradiol*. 2005;26(4):725–729.
- Hasan KM, Walimuni IS, Kramer LA, Narayana PA. Human brain atlas-based volumetry and relaxometry: application to healthy development and natural aging. *Magn Reson Med*. 2010;64(5):1382–1389.
- Kumar R, Delshad S, Woo MA, Macey PM, Harper RM. Age-related regional brain T<sub>2</sub>-relaxation changes in healthy adults. *J Magn Reson Imaging*. 2012;35(2):300–308.
- Wang J, Shaffer ML, Eslinger PJ, Sun X, Weitekamp CW, Patel MM, Dossick D, Gill DJ, Connor JR, Yang QX. Maturational and aging effects on human brain apparent transverse relaxation. *PLoS ONE*. 2012;7(2):e31907.
- Decarli C, Murphy DG, Gillette JA, Haxby JV, Teichberg D, Schapiro MB, Horwitz B. Lack of age-related differences in temporal lobe volume of very healthy adults. *AJNR Am J Neuroradiol*. 1994;15(4):689–696.
- Raz N, Gunning FM, Head D, Dupuis JH, McQuain J, Briggs SD, Loken WJ, Thornton AE, Acker JD. Selective aging of the human cerebral cortex observed *in vivo*: differential vulnerability of the prefrontal gray matter. *Cereb Cortex*. 1997;7(3):268–282.
- O'Sullivan M, Jones DK, Summers PE, Morris RG, Williams SC, Markus HS. Evidence for cortical "disconnection" as a mechanism of age-related cognitive decline. *Neurology*. 2001;57(4):632–638.
- Resnick SM, Pham DL, Kraut MA, Zonderman AB, Davatzikos C. Longitudinal magnetic resonance imaging studies of older adults: a shrinking brain. *J Neurosci*. 2003;23(8):3295–3301.

38. Ota M, Obata T, Akine Y, Ito H, Asada T, Suhara T. Age-related degeneration of corpus callosum measured with diffusion tensor imaging. *Neuroimage*. 2006; 31(4):1445–1452.
39. Kim EY, Kim DH, Yoo E, Park HJ, Golaxy X, Lee SK, Kim DJ, Kim J, Kim DI. Visualization of maturation of the corpus callosum during childhood and adolescence using T2 relaxometry. *Int J Dev Neurosci*. 2007;25(6):409–414.
40. Lebel C, Caverhill-godkewitsch S, Beaulieu C. Age-related regional variations of the corpus callosum identified by diffusion tensor tractography. *Neuroimage*. 2010;52(1):20–31.
41. Hasan KM, Walimuni IS, Abid H, Frye RE, Ewing-Cobbs L, Wolinsky JS, Narayana PA. Multimodal quantitative magnetic resonance imaging of thalamic development and aging across the human lifespan: implications to neurodegeneration in multiple sclerosis. *J Neurosci*. 2011;31(46):16826–16832.
42. Hasan KM, Walimuni IS, Kramer LA, Narayana PA. Human brain iron mapping using atlas-based T2 relaxometry. *Magn Reson Med*. 2012;67(3):731–739.
43. Hallgren B, Sourander P. The effect of age on the non-haemin iron in the human brain. *J Neurochem*. 1958;3(1):41–51.
44. Tosk JM, Holshouser BA, Aloia RC, Hinshaw DB, Hasso AN, Macmurray JP, Will AD, Bozzetti LP. Effects of the interaction between ferric iron and L-dopa melanin on T1 and T2 relaxation times determined by magnetic resonance imaging. *Magn Reson Med*. 1992;26(1):40–45.
45. Gelman N, Gorell JM, Barker PB, Savage RM, Spickler EM, Windham JP, Knight RA. MR imaging of human brain at 3.0 T: preliminary report on transverse relaxation rates and relation to estimated iron content. *Radiology*. 1999;210(3):759–767.
46. Ding XQ, Kucinski T, Wittkugel O, Goebell E, Grzyska U, Görg M, Kohlschütter A, Zeumer H. Normal brain maturation characterized with age-related T2 relaxation times: an attempt to develop a quantitative imaging measure for clinical use. *Invest Radiol*. 2004;39(12):740–746.
47. Bilgic B, Pfefferbaum A, Rohlfing T, Sullivan EV, Adalsteinsson E. MRI estimates of brain iron concentration in normal aging using quantitative susceptibility mapping. *Neuroimage*. 2012;59(3):2625–2635.
48. Lambert C, Chowdhury R, Fitzgerald TH, Fleming SM, Lutti A, Hutton C, Draganski B, Frackowiak R, Ashburner J. Characterizing aging in the human brainstem using quantitative multimodal MRI analysis. *Front Hum Neurosci*. 2013;7:462.
49. Fearnley JM, Lees AJ. Ageing and Parkinson's disease: substantia nigra regional selectivity. *Brain*. 1991;114(Pt 5):2283–2301.
50. Zecca L, Gallorini M, Schünemann V, Trautwein AX, Gerlach M, Riederer P, Vezoni P, Tampellini D. Iron, neuromelanin and ferritin content in the substantia nigra of normal subjects at different ages: consequences for iron storage and neurodegenerative processes. *J Neurochem*. 2001;76(6):1766–1773.
51. Ogg RJ, Steen RG. Age-related changes in brain T<sub>1</sub> are correlated with iron concentration. *Magn Reson Med*. 1998;40(5):749–753.
52. Cowell PE, Turetsky BI, Gur RC, Grossman RI, Shtasel DL, Gur RE. Sex differences in aging of the human frontal and temporal lobes. *J Neurosci*. 1994;14(8):4748–4755.
53. Gur RC, Mozley PD, Resnick SM, Gottlieb GL, Kohn M, Zimmerman R, Herman G, Atlas S, Grossman R, Berretta D. Gender differences in age effect on brain atrophy measured by magnetic resonance imaging. *Proc Natl Acad Sci USA*. 1991;88(7):2845–2849.
54. Lemaître H, Crivello F, Grassiot B, Alperovitch A, Tzourio C, Mazoyer B. Age- and sex-related effects on the neuroanatomy of healthy elderly. *Neuroimage*. 2005;26(3):900–911.
55. Inano S, Takao H, Hayashi N, Abe O, Ohtomo K. Effects of age and gender on white matter integrity. *AJNR Am J Neuroradiol*. 2011;32(11):2103–2109.
56. Coffey CE, Lucke JF, Saxton JA, Ratcliff G, Unitas LJ, Billig B, Bryan RN. Sex differences in brain aging: a quantitative magnetic resonance imaging study. *Arch Neurol*. 1998;55(2):169–179.
57. Gur RE, Gur RC. Gender differences in aging: cognition, emotions, and neuroimaging studies. *Dialogues Clin Neurosci*. 2002;4(2):197–210.
58. Berchtold NC, Cribbs DH, Coleman PD, Rogers J, Head E, Kim R, Beach T, Miller C, Troncoso J, Trojanowski JQ, Zielke HR, Cotman CW. Gene expression changes in the course of normal brain aging are sexually dimorphic. *Proc Natl Acad Sci USA*. 2008;105(40):15605–15610.
59. Kawata M. Roles of steroid hormones and their receptors in structural organization in the nervous system. *Neurosci Res*. 1995;24(1):1–46.
60. Goldstein JM, Seidman LJ, Horton NJ, Makris N, Kennedy DN, Caviness VS, Jr, Faraone SV, Tsuang MT. Normal sexual dimorphism of the adult human brain assessed by in vivo magnetic resonance imaging. *Cereb Cortex*. 2001;11(6):490–497.
61. Phillips OR, Clark KA, Luders E, Azhir R, Joshi SH, Woods RP, Mazziotta JC, Toga AW, Narr KL. Superficial white matter: effects of age, sex, and hemisphere. *Brain Connect*. 2013;3(2):146–159.
62. Sun T, Walsh CA. Molecular approaches to brain asymmetry and handedness. *Nat Rev Neurosci*. 2006;7(8):655–662.
63. Good CD, Johnsrude I, Ashburner J, Henson RN, Friston KJ, Frackowiak RS. Cerebral asymmetry and the effects of sex and handedness on brain structure: a voxel-based morphometric analysis of 465 normal adult human brains. *Neuroimage*. 2001;14(3):685–700.
64. Westerhausen R, Kreuder F, Sequeira SDS, Walter C, Woerner W, Wittling RA, Schweiger E, Wittling W. Effects of handedness and gender on macro- and microstructure of the corpus callosum and its subregions: a combined high-resolution and diffusion-tensor MRI study. *Brain Res Cogn Brain Res*. 2004;21(3):418–426.
65. Büchel C, Raedler T, Sommer M, Sach M, Weiller C, Koch MA. White matter asymmetry in the human brain: a diffusion tensor MRI study. *Cereb Cortex*. 2004;14(9):945–951.
66. Li M, Chen H, Wang J, Liu F, Wang Y, Lu F, Yu C, Chen H. Increased cortical thickness and altered functional connectivity of the right superior temporal gyrus in left-handers. *Neuropsychologia*. 2015;67:27–34.
67. Häberling IS, Badzakova-trajkova G, Corballis MC. Callosal tracts and patterns of hemispheric dominance: a combined fMRI and DTI study. *Neuroimage*. 2011; 54(2):779–786.
68. Chepur NB, Yen YF, Burdette JH, Li H, Moody DM, Maldjian JA. Diffusion anisotropy in the corpus callosum. *AJNR Am J Neuroradiol*. 2002;23(5):803–808.
69. Fabri M, Pierpaoli C, Barbaresi P, Polonara G. Functional topography of the corpus callosum investigated by DTI and fMRI. *World J Radiol*. 2014;6(12):895–906.
70. Herrero MT, Barcia C, Navarro JM. Functional anatomy of thalamus and basal ganglia. *Childs Nerv Syst*. 2002;18(8):386–404.
71. Vrenken H, Geurts JJ, Knol DL, van Dijk LN, Dattola V, Jasperse B, van Schijndel RA, Polman CH, Castelijns JA, Barkhof F. Whole-brain T<sub>1</sub> mapping in multiple sclerosis: global changes of normal-appearing gray and white matter. *Radiology*. 2006;240(3):811–820.
72. Lim, SY. T<sub>1</sub> relaxometry of the thalamus in clinically isolated syndrome using 7 Tesla MRI. Abstract presented at: 25th Congress of the European Committee for the Treatment and Research in MS; October 9-12, 2009; Dusseldorf, Germany.
73. Ma D, Pierre EY, Jiang Y, Setsompop K, Gulani V, Griswold MA. Three-dimensional MR fingerprinting (MRF) and MRF-music acquisitions. *Proc Intl Soc Mag Reson Med*. 23 (2015). Abstract no. 3390.
74. Ma D, Pierre EY, Jiang Y, Schluchter MD, Setsompop K, Gulani V, Griswold MA. Music-based magnetic resonance fingerprinting to improve patient comfort during MRI examinations. *Magn Reson Med*. 2015 July 6; doi: 10.1002/mrm.25818.
75. Jiang Y, Ma D, Seiberlich N, Gulani V, Griswold MA. MR fingerprinting using fast imaging with steady state precession (FISP) with spiral readout. *Magn Reson Med*. 2014 Dec 9; doi: 10.1002/mrm.25559.